Available online at www.sciencedirect.com
ScienceDirect
Trans. Nonferrous Met. Soc. China 31(2021) 3096−3104
Transactions of Nonferrous Metals Society of China
www.tnmsc.cn

Macrosegregation and thermosolutal convection-related freckle formation in directionally solidified Sn−Ni peritectic alloy in crucibles with different diameters

Peng PENG[1,2,3], Sheng-yuan LI[1*], Wan-chao ZHENG[1*], Li LU[1], Shu-dong ZHOU[1]

1. School of Materials and Energy, Lanzhou University, Lanzhou 730000, China;
2. Key Laboratory for Magnetism and Magnetic Materials of the Ministry of Education, Lanzhou University, Lanzhou 730000, China;
3. Northwest Rare Metal Materials Research Institute, Shizuishan 753000, China;

Received 22 October 2020; accepted 23 June 2021

Abstract: Different from other alloys, the observation in this work on the dendritic mushy zone shows that the freckles are formed in two different regions before and after peritectic reaction in directional solidification of Sn−Ni peritectic alloys. In addition, the experimental results demonstrate that the dendritic morphology is influenced by the temperature gradient zone melting and Gibbs−Thomson effects. A new Rayleigh number (Ra_P) is proposed in consideration of both effects and peritectic reaction. The prediction of Ra_P confirms the freckle formation in two regions during peritectic solidification. Besides, heavier thermosolutal convection in samples with larger diameter is also demonstrated.

Key words: freckle formation; directional solidification; thermosolutal convection; dendritic solidification; Sn−Ni peritectic alloy

1 Introduction

Among numerous solidification methods, directional solidification is frequently applied, especially in different metallic systems [1−6]. During directional solidification of alloys with a freezing range, the formation of defects like freckle can be initiated by localized thermosolutal convection in a mushy zone [4−9]. As a persistent and challenging problem, freckles are usually composed of small chains of dendrite fragments and pores along the direction of solidification. In upward directional solidification, the temperature profile is assumed to stabilize against thermosolutal convection [3], while the solutal profile is destabilized when the rejected solute can decrease the density of the melt [10−14], leading to a liquid-density inversion and thermosolutal convection.

To quantify the longitudinal thermosolutal convection in the dendritic mushy zone, the mushy zone Rayleigh number Ra has been proven to be an useful parameter to predict freckle formation. There are several definitions of Ra, and the onset of thermosolutal convection has been suggested to result in freckle formation if Ra exceeds a critical value [10−14]. Ra is directly determined by the permeability K which is dependent on the solid volume fraction (f_S) and the specific surface area of dendrites in commonly encountered dendritic structure [15−17]. Thus, the details of the dendritic structure can strongly influence the permeability K and Ra. As a result, the evolution of the dendritic mushy zone during the solidification should be

Corresponding author: Peng PENG, Tel: +86-931-2166588, E-mail: pengp@lzu.edu.cn
*Sheng-yuan LI and Wan-chao ZHENG contributed equally to this work
DOI: 10.1016/S1003-6326(21)65718-7

reasonably described, which is still insufficient.

As a matter of fact, the evolution of the dendritic structure can be brought about by different effects. The Gibbs−Thomson (G−T) effect driven coarsening process can give rise to diffusion in melt between adjacent secondary branches if their radii are different [7−9], resulting in remelting on the thinner secondary branches and resolidification on the thicker secondary branches. Besides, solute diffusion in the melt can also be brought about by the temperature gradient during solidification [18], which is termed as temperature gradient zone melting (TGZM) [18−21]. During past decades, dendritic growth has been witnessed in numerous important peritectic alloys, like Fe–Ni and steel alloys [22]. The restriction of the coarsening process by peritectic reaction was confirmed [9] while the promotion of the TGZM effect has also been proved [23] during peritectic solidification. In addition, TURKELI [24] also proposed that the TGZM effect could play a more important role in dendrite evolution as compared with the Gibbs−Thomson effect. Nevertheless, the analysis on the evolution of dendritic mushy zone during the peritectic solidification which is associated with fluid flow has not been performed yet.

As mentioned above, despite the importance of prediction of freckle formation during solidification, current analysis on peritectic alloys which have been widely applied has not been performed yet. In addition, it has been confirmed that thermosolutal convection is obviously influenced by the diameter of the sample [25,26], which could give rise to a wide variety of microstructures in directionally solidified peritectic samples of different diameters. The dependence of heavier thermosolutal convection on larger sample diameter has been confirmed by previous researches [25−28]. However, the prediction of the influence of the melt convection on microstructure development is not adequate since the evolution of dendritic structure by both the TGZM and G−T effects has not been taken into account before. Therefore, based on an analytical model describing the permeability K in consideration of both effects, a new Rayleigh number Ra_P for dendritic solidification is proposed in this work. This new Rayleigh number Ra_P is proved to be capable of predicting freckle formation in dendritic solidification of peritectic alloys.

2 Experimental

The as-cast Sn−36at.%Ni alloy was firstly induction melted by nickel and tin with purity of 99.9%. Then, the rods (d(1, 2, 3.5) mm×110 mm) were cut from the ingot. Firstly, the rod was placed into the Al_2O_3 tube. Secondly, the temperature of the rod was raised to 1250 °C to melt it. Thirdly, after the sample has been kept still for 30 min, directional growth was performed at the same growth velocity of 5 μm/s by pulling the sample. Fourthly, the crucible was quenched into liquid Ga−In−Sn alloy when a growth distance of 40 mm was reached. The temperature gradient was measured by the PtRh30-PtRh6 thermocouple in the alumina crucible interface, and was approximately 42 K/mm at the solid/liquid interface. Finally, both the longitudinal and transversal views of the samples were captured by scanning electron microscopy (SEM (Quanta−200)).

3 Results

Figures 1(a−c) give the entire structure from quenched solid/liquid interface at liquidus temperature T_L (1040 °C) to the peritectic reaction interface at peritectic reaction temperature T_P (798 °C). It can be observed that the line defects which are composed of equiaxed grains and porosity can be seen from these macroscopic views. This line defect proves the formation of freckles during directional solidification since freckle is composed of a chains of equiaxed grains or dendrite fragments along the solidification direction [29]. In addition, in contrast to other kinds of alloys, freckles can be witnessed in two different regions: Region I between T_L and T_P and Region II below T_P. The local microstructures in Regions I and II are presented in Figs. 1(a_1−c_1) and (a_2−c_2), respectively. According to the EDS result, the dark grey phase is Ni_3Sn_2 phase, the light grey one is Ni_3Sn_4 phase, and the white one is the remaining liquid [23].

In addition, the examination on Fig. 1 shows that fewer freckles can be found in sample with smaller diameter. The observations from the longitudinal sections in Figs. 1(a_1−c_1) and (c_2−c_2) are consistent with those from the transversal sections in Figs. 1(d−f). The distance between the transversal sections to the peritectic reaction

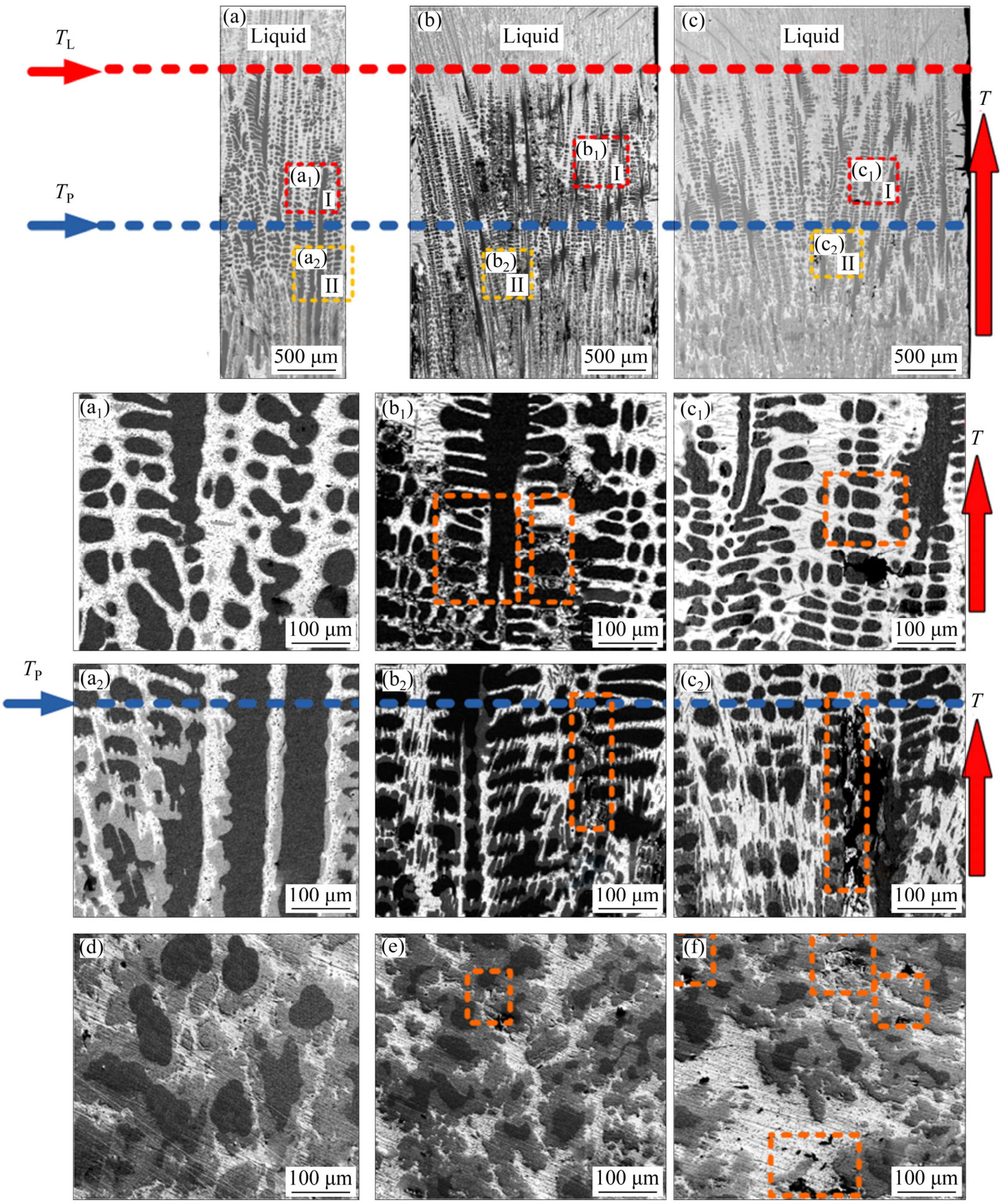

Fig. 1 Typical microstructures of freckles in dendritic mushy zone of Sn−36at.%Ni peritectic alloys: (a−c) Macrostructures at diameter d values of 1 mm (a), 2 mm (b) and 3.5 mm (c); (a_1−c_1) Microstructures showing freckle formation in Region I at d values of 1 mm (a_1), 2 mm (b_1) and 3.5 mm (c_1) between T_L and T_P; (a_2−c_2) Microstructures showing freckle formation in Region II at d values of 1 mm (a_2), 2 mm (b_2) and 3.5 mm (c_2) below T_P; (d−f) Microstructures showing freckle formation at d values of 1 mm (d), 2 mm (e) and 3.5 mm (f) below T_P from transversal sections of samples

interface at T_P is 500 μm. To quantify the dependence of the freckle formation in the samples on their diameters, Table 1 is presented to show the distribution of the freckles from both the longitudinal and transversal sections. The effectiveness of the G−T effect can be determined due to the secondary branches with different radii. In addition, the examination on Figs. 1(a_2−c_2) also show the partial enclosure of peritectic Ni_3Sn_4 phase on the front edge of primary Ni_3Sn_2 phase, confirming the effectiveness of the TGZM effect in peritectic alloy [18,19,21,23]. Thus, the effects of the dendritic mushy zone will be analyzed as follows.

Table 1 Numbers of freckles in different sections of directionally solidified Sn−36at.%Ni peritectic alloys with different diameters

Sample diameter, d/mm	Number of freckles		
	Region I, longitudinal	Region II, longitudinal	Region II, transversal
1	0	0	1
2	8	6	8
3.5	10	8	9

4 Discussion

4.1 Melt macrosegregation in mushy zone

In the present work, the rejected Sn continuously decreases the density of the melt, leading to solute redistribution and following macrosegregation in the mushy zone. The composition of the longitudinal sections is determined through the EDS method. A specific composition result is obtained from averaging the 6 EDS results measured from the same distance from the quenched solid/liquid interface. In addition, the solid volume fraction f_S is determined by directly measuring on the longitudinal sections. Thus, the longitudinal macrosegregation measured in these samples with different diameters are given in Fig. 2(a). This indicates that the longitudinal macrosegregation increases as the diameter d increases. Furthermore, the actual (effective) solute distribution coefficient also changes in the presence of thermosolutal convection in the mushy zone. The $\lg(C_L/C_0)$ vs $\lg(1-f_S)$ curve is plotted in Fig. 2(b), where C_L is the melt concentration, C_0 is the initial concentration of the alloy and based on the relationship $C_L/C_0=(1-f_S)^{k_e-1}$, the linear fit through the data is k_e-1. Therefore, the macrosegregation data show that k_e (obtained from the slope of the data) is smaller when the diameter is smaller, indicating that the influence of the thermosolutal convection is more significant when d is larger. It should be noted that the same trend cannot be obtained using the Lever-rule from equilibrium phase diagram, which is based on equilibrium diffusion condition.

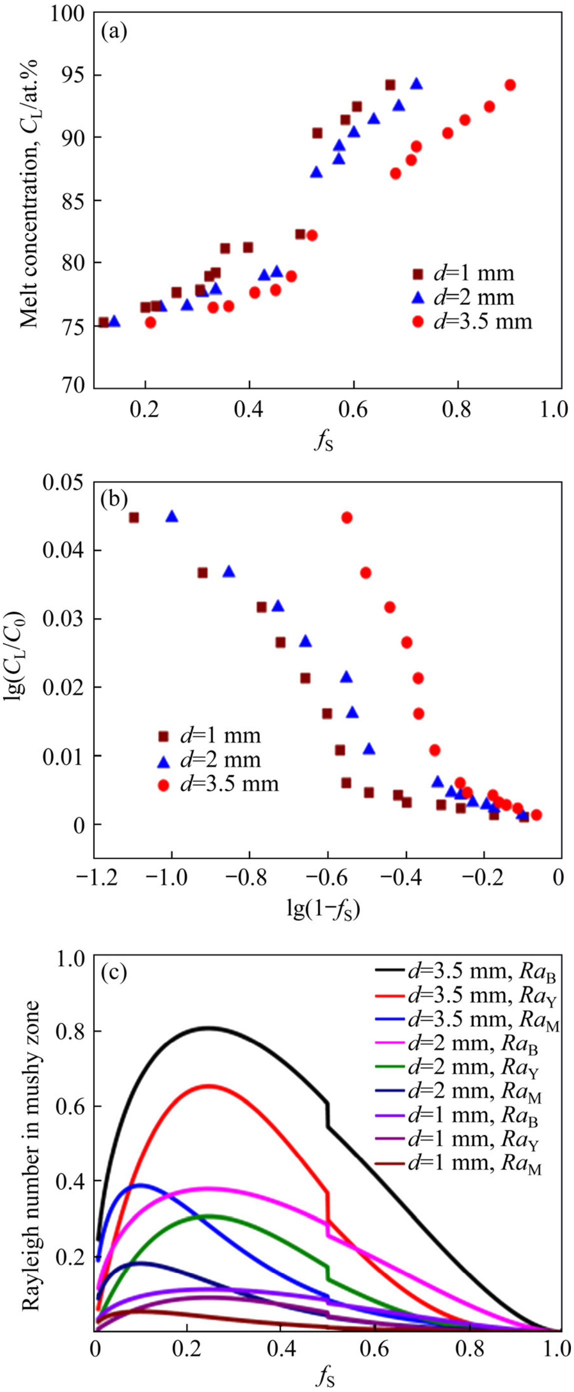

Fig. 2 Macrosegregation in directionally solidified Sn−36at.%Ni peritectic alloys with different diameters: (a) Melt concentration as function of fraction of solid phase f_S; (b) $\lg(C_L/C_0)$ vs $\lg(1-f_S)$ plot showing macrosegregation; (c) Dependences of Rayleigh numbers Ra_B, Ra_Y and Ra_M on f_S at growth velocity of 5 μm/s

Although Ra provides a reliable method to evaluate freckle formation [3], many versions of it can be found in Ref. [12−14]. BECKERMANN et al [14] stated that the following definition was most effective in predicting freckle formation:

$$Ra=\left(\Delta\rho/\rho_0\right)\frac{gK}{\alpha\nu} \tag{1}$$

$$\Delta\rho/\rho_0=\left(\rho_0-\rho(h)\right)/\rho_0 \tag{2}$$

where $\Delta\rho/\rho_0$ is the liquid-density inversion term in the mushy zone, g is the gravity acceleration, α is the thermal diffusivity, ν is the kinematic viscosity, ρ_0 is the density of the melt above the quenched solid/liquid interface, and $\rho(h)$ is the density of the melt as a function of the height (h). With regards to the permeability K, they are assumed [14]:

$$K_{\mathrm{B}}=6\times10^{-4}\lambda_1^2\left[\left(1-f_{\mathrm{S}}\right)^3/f_{\mathrm{S}}^2\right] \tag{3}$$

and YANG et al [12] used K as

$$K_{\mathrm{Y}}=3.75\times10^{-4}\lambda_1^2\left(1-f_{\mathrm{S}}\right)^2 \tag{4}$$

where λ_1 is the dendritic spacing.

After that, in consideration of the influence of the secondary branches on permeability, TEWARI et al [13] proposed that

$$K_{\mathrm{M}}=\frac{\left(1-f_{\mathrm{S}}\right)^3}{4.2S_V^2f_{\mathrm{S}}^2} \tag{5}$$

$$S_V=\frac{\left[3.38-3.29\left(1-f_{\mathrm{S}}\right)+8.85\left(1-f_{\mathrm{S}}\right)^2\right]}{\lambda_1\left[\dfrac{D_{\mathrm{L}}Gk}{Vm_{\mathrm{L}}C_0\left(k-1\right)}\right]} \tag{6}$$

where V is the growth velocity, m_{L} is the liquidus slope of the solid phase, C_0 is the initial composition of the alloy, D_{L} is the solute diffusion coefficient, G is the temperature gradient and k is the solute distribution coefficient. Based on Eqs. (1) to (6), the Rayleigh numbers obtained are defined as Ra_{B} [14], Ra_{Y} [12] and Ra_{M} [13], respectively.

The predictions from different definitions of the Rayleigh number mentioned above at V=5 μm/s with different diameters are given in Fig. 2 from f_{S} of 0.01 to 0.9, and f_{S} is related to melt concentration C_{L} [30]. The maximum values can be observed in all predictions, and the sudden decrease of mushy zone Rayleigh number Ra when f_{S} is 0.51 corresponds to the occurrence of peritectic reaction. A maximum value can be observed because the permeability decreases while the density inversion increases with the increase of f_{S} [14]. Since the freckles by thermosolutal convection are formed if Ra exceeds a critical value [12−14], the freckles are formed when Ra is close to the maximum value. However, different from the unique maximum in previous reports, the freckles are observed in two different regions in Fig. 1(c), indicating that two local maximums of Ra should exist during directional solidification of peritectic alloys. However, this cannot be predicted through the current definitions of Ra. Therefore, a new definition of Ra will be developed in this work to solve this problem.

Since the validity of the definition of the mushy zone Rayleigh number through Eq. (1) has been carried out in numerous researches, the new expression of the mushy zone Rayleigh number in this work should also be consistent with it. The investigation on Eq. (1) shows that the new development of Rayleigh number can only be achieved through the permeability of the mushy zone K for a specific alloy system, which is the same as those in previous works [12−14]. Thus, the evolution of dendritic structure which determines the permeability K in peritectic system is firstly analyzed.

4.2 Evolution of dendritic mushy zone

To compare with the previous coarsening models [6−9], as exhibited in Figs. 3−6, a thinner branch is assumed to be at the intermediate temperature. This is because the remelting/ resolidification processes on the thinner secondary branch are complex. The remelting process on the back edge and resolidification process on the front edge can be induced by the TGZM effect. However, the remelting process by the G−T effect can take place on both edges. Furthermore, the solute fluxes induced by both effects are assumed to be independent for simplicity. In order to compare these effects, the melt concentration difference ΔC by these effects is used here since lager ΔC can lead to larger remelting/resolidification velocities and more obvious influence on the evolution of dendritic structure.

Based on the experimental examination, Figs. 3−6 illustrate that the evolution process of dendritic structure by both effects can be divided into four successive stages. Only α phase participates in Stage I before peritectic reaction in Fig. 3. The equilibrium liquidus of α phase is the

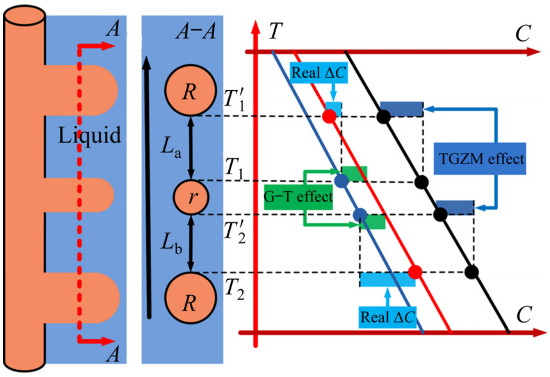

Fig. 3 Illustration of remelting/resolidification processes during directional solidification of peritectic alloy in Stage I

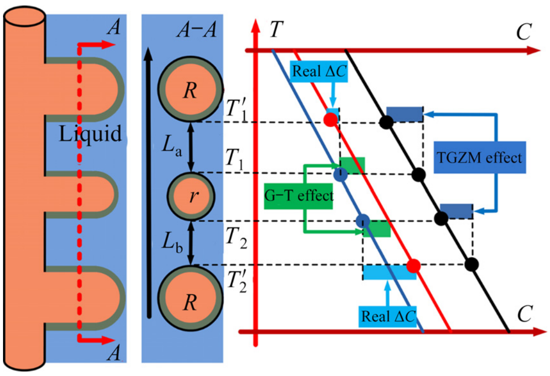

Fig. 4 Illustration of remelting/resolidification processes during directional solidification of peritectic alloy in Stage II

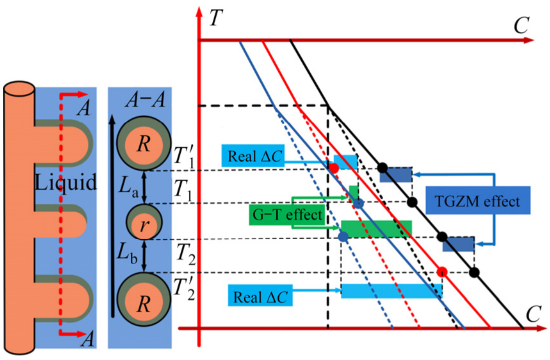

Fig. 5 Illustration of remelting/resolidification processes during directional solidification of peritectic alloy in Stage III

black line, and the other two liquidus lines with radii of r and R are also given. It can be observed from Fig. 3 that ΔC by the TGZM effect is larger than that by the G−T effect at both the front (T_1) and back (T_2) edges. The real ΔC is the sum of ΔC by both effects. Therefore, the comparison between the real ΔC at T_1 and T_2 indicates that the remelting velocity at T_2 is larger than the resolidification velocity at T_1.

Stage II initiates that below T_P, only β phase is taken into account in this stage. Figure 4 confirms that ΔC by the G−T effect is also smaller than that by TGZM effect at both T_1 and T_2. Therefore, r gradually decreases. Then, Stage III can take place when the β phase at T_2 completely remelts first. The dashed lines in Fig. 5 are the extension of the equilibrium liquidus lines of α phase. The thinner secondary branch will be composed of β phase as directional solidification proceeds. Stage III is finished when β phase at T_1' completely remelts. As a result, as displayed in Fig. 6, β appears at T_1'. Stage IV is finished when this thinner branch disappears.

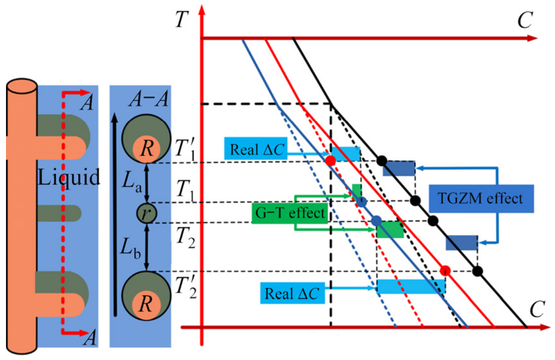

Fig. 6 Illustration of remelting/resolidification processes during directional solidification of peritectic alloy in Stage IV

4.3 Prediction of freckle formation through current Rayleigh number

The establishment of the analytical model on the permeability K based on the remelting/resolidification process is illustrated in Figs. 3−6. Based on the theoretical prediction of the permeability K, the dependence of the mushy zone Rayleigh number on the volume fraction of solidified phase f_S is given in Fig. 7. To show the difference between the present work and previous works [12−14], the Rayleigh number defined in this work is Ra_P. The increase of Ra_P with increasing sample diameter is consistent with the previous reports [10−14,25,26] that the thermosolutal convection is heavier when the diameter of the sample is larger.

The most special feature of the present prediction of Ra_P is that two maximum values can be found: one before peritectic reaction and the

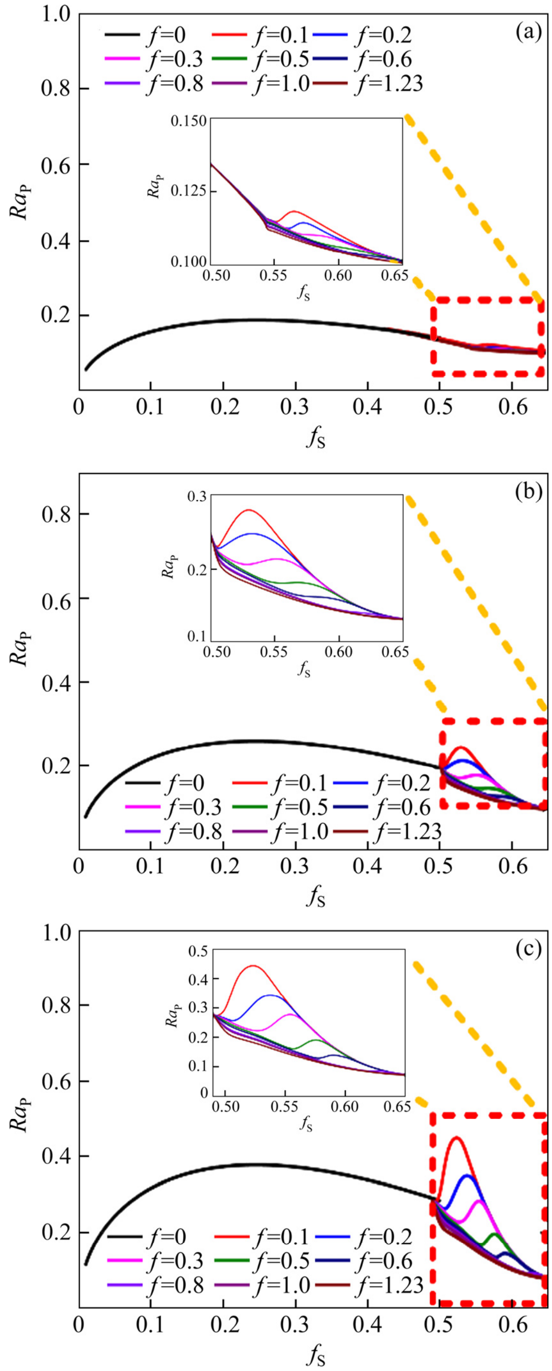

Fig. 7 Dependences of mushy zone Rayleigh number Ra_P on fraction of solid phase f_S at different diameters of sample: (a) 1 mm; (b) 2 mm; (c) 3.5 mm

other after peritectic reaction. In addition, although the first maximum is always larger than the second one, both maximum values increase with increasing sample diameter, and the second maximum values nearly disappear when the diameter is 1 mm. The enlarged views of the second maximum values are also illustrated to improve the understanding of the variation of Ra_P. The enlarged views confirm that the solid fraction f_S values corresponding to these maximums are consistent with the experimental results. The degree of peritectic reaction is characterized by a reaction constant f which is defined as the ratio of the thickness of the peritectic layer (δr) formed during peritectic reaction to the initial thin-arm radius (r_p) before peritectic reaction. Since freckle formation is the most possible if Rayleigh number reaches the maximum [14−16], it can therefore be concluded that the two different regions where freckle formation can be observed correspond to these two maximum values of the Rayleigh number Ra_P.

However, it is worth noting that although the second maximum is always smaller than the first one, the freckles can still be found below T_P. This indicates that the freckle formation depends on not only the absolute magnitude but also the relative magnitude of the Rayleigh number in local regions. Furthermore, it should be reiterated that the formation mechanisms of the freckles at these two different regions are different. In Region I which is formed before peritectic reaction, a maximum of Ra_P can be observed because the permeability decreases while the density inversion increases with f_S [14]. In addition, the maximum of Ra_P in Region II which is formed after peritectic reaction can be attributed to the obvious increase of permeability K due to the combined influences of the G−T and TGZM effects during peritectic solidification. Therefore, it can be confirmed from the analysis above that the details of the dendritic structure can strongly influence the thermosolutal convection.

5 Conclusions

(1) Different from other types of alloys, the freckles are formed in two different regions during directional solidification of peritectic alloys.

(2) More freckles can be found in samples of larger diameter. Only Region I can be explained by the current theories on Rayleigh number Ra predicting freckle formation by thermosolutal convection through the maximum of Ra.

(3) Both the TGZM and G−T effects are closely related to dendrite morphology during directional solidification. Ra_P is proposed in consideration of both effects, and Ra_P not only exhibits a maximum value after peritectic reaction but also confirms heavier thermosolutal convection in larger samples.

Acknowledgments

Authors thank to the financial supports from the National Natural Science Foundation of China (No. 51871118), the Basic Scientific Research Business Expenses of the Central University and Open Project of Key Laboratory for Magnetism and Magnetic Materials of the Ministry of Education, Lanzhou University, China (No. LZUMMM2021005), the Science and Technology Project of Lanzhou City, China (No. 2019-1-30), and the State Key Laboratory of Special Rare Metal Materials, China (No. SKL2020K003).

References

[1] YANG Yong, FENG He-ping, WANG Qi, CHEN Rui-run, GUO Jing-jie, DING Hong-sheng, SU Yan-qing. Improvement of microstructure and mechanical properties of TiAl−Nb alloy by adding Fe element [J]. Transactions of Nonferrous Metals Society of China, 2020, 30: 1315−1324.

[2] ZHANG Yu, JING Hong-yang, XU Lian-yong, HAN Yong-dian, ZHAO Lei, LI Hai-zhou, TANG Zheng-xin, TONG Tian-wang. Microstructure and grain boundary engineering of a novel Fe−Cr−Ni alloy weldment made with self-developed composition-matched weld filler metal [J]. Transactions of Nonferrous Metals Society of China, 2020, 30: 992−1004.

[3] LANG Yuan, LEE P D. A new mechanism for freckle initiation based on microstructural level simulation [J]. Acta Materialia, 2012, 60: 4917−4926.

[4] ZHOU Can-xu, LIU Yuan, ZHANG Hua-wei, CHEN Xiang, LI Yan-xiang. Fabrication of lotus-type porous Mg−Mn alloys by metal/gas eutectic unidirectional solidification [J]. Transactions of Nonferrous Metals Society of China, 2020, 30: 1524−1534.

[5] MADISON J, SPOWART J E, ROWENHORST D J, AAGESEN L K, THORNTON K, POLLOCK T M. Fluid flow and defect formation in the three-dimensional dendritic structure of nickel-based single crystals [J]. Metallurgical Materials Transactions, 2012, 43: 369−380.

[6] PLOTKOWSKIl A, M KRANE M J. On the numerical prediction of channel segregation [J]. International Journal of Heat and Mass Transfer, 2016, 100: 11−23.

[7] MARSH S P, GLICKSMAN M E. Overview of geometric effects on coarsening of mushy zones [J]. Metallurgical Materials Transactions A, 1996, 27: 557−567.

[8] COUGHLIN J C, KATTAMIS T Z, FLEMINGS M C. Influence of coarsening on dendrite arm spacing of aluminum−copper alloys [J]. Transactions AIME, 1967, 239: 1504−1511.

[9] MA D, XU W, NG S C, LI Y. On secondary dendrite arm coarsening in peritectic solidification [J]. Materials Science and Engineering A, 2005, 390: 52−62.

[10] AUBRTIN P, WANG T, COCKCRFT S L, MITCHELL A. Freckle formation and freckle criterion in superalloy castings [J]. Metallurgical Materials Transactions B, 2000, 31: 801−811.

[11] EMMS P W. Freckle formation in a solidifying binary alloy [J]. Journal of Engineering Mathematics, 1998, 33: 175−200.

[12] YANG Wan-hong, CHEM Wei, CHANG K M, MANNAN S, DEBARBDILLO J. Freckle criteria for the upward directional solidification of alloys [J]. Metallurgical Materials Transactions A, 2001, 32: 397−406.

[13] TEWARI S N, TIWARI R, MGADI G. A mushy-zone Rayleigh number to describe macrosegregation and channel segregate formation during directional solidification of metallic alloys [J]. Metallurgical Materials Transactions A, 2004, 35: 2927−2933.

[14] BECKERMANN C, GU J P, BOETTINGER W J. Development of a freckle predictor via Rayleigh number method for single-crystal nickel-base superalloy castings [J]. Metallurgical Materials Transactions A, 2000, 31: 2545−2557.

[15] SUN Dong-ke, XING Hui, DONG Xiang-lei, HAN Yong-sheng. An anisotropic lattice Boltzmann-phase field scheme for numerical simulations of dendritic growth with melt convection [J]. International Journal of Heat and Mass Transfer, 2019, 133: 1240−1250.

[16] KHAJEH E, MAIJER D M. Permeability of dual structured hypoeutectic aluminum alloys [J]. Acta Materialia, 2011, 59: 4511−4524.

[17] YANG Bei, WANG Zhi-feng. Image-based modelling for fluid flow and permeability prediction within continuously-evolving mushy zone during melting and solidification [J]. International Journal of Heat and Mass Transfer, 2020, 147: 119234-1−119234-9.

[18] RETTENMAYR M. Melting and remelting phenomena [J]. International Materials Reviews, 2009, 54: 1−17.

[19] LIU Dong-mei, LI Xin-zhong, SU Yan-qing, PENG Peng, LUO Liang-shun, GUO Jing-jie, FU Heng-zhi. Secondary dendrite arm migration caused by temperature gradient zone melting during peritectic solidification [J]. Acta Materialia, 2012, 60: 2679−2688.

[20] PHILLION A B, ZALOZNIK M, SPINDLER I, PINTER N, ALEDO C A, SALLOUM ABOU JAOUDE G, NGUYEN H. Evolution of a mushy zone in a static temperature gradient using a volume average approach [J]. Acta Materialia, 2017, 141: 206−216.

[21] PAN Shi-yan, ZHANG Qing-yu, ZHU Ming-fang, RETTENMAYR M. Liquid droplet migration under static and dynamic conditions: Analytical model, phase-field simulation and experiment [J]. Acta Materialia, 2015, 86: 229−239.

[22] KERR H W, KURZ W. Solidification of peritectic alloys [J]. International Materials Reviews, 1996, 41: 129−164.

[23] PENG Peng, LI Xin-zhong, SU Yan-qing, GUO Jing-jie, FU Heng-zhi. Microsegregation of peritectic systems in a temperature gradient: Analysis in directionally solidified Sn−36at.%Ni peritectic alloy [J]. International Journal of Heat and Mass Transfer, 2016, 94: 488−497.

[24] TURKELI A. Simple analytical models for dendrite arm coarsening under high and medium temperature gradients [J]. Materials Science Forum, 2006, 508: 331−336.

[25] PARK J S, TRIVEDI R. Convection-induced novel

oscillating microstructure formation in peritectic systems [J]. Journal of Crystal Growth, 1998, 187: 511−515.

[26] MAZUMDER P, TRIVEDI R, KARMA A. A model of convection-induced oscillatory structure formation in peritectic alloys [J]. Metallurgical Materials Transactions A, 2000, 31: 1233−1246.

[27] LONG Ping, WANG Guan-shi, TIAN Jun, HU Shi-li, LUO Si-hai. Simulation of one-dimensional column leaching of weathered crust elution-deposited rare earth ore [J]. Transactions of Nonferrous Metals Society of China, 2019, 29: 625−633.

[28] CHEN Zhong-wei, GAO Jian-ping. Formation of twinned dendrites during unidirectional solidification of Al−32%Zn alloy [J]. Transactions of Nonferrous Metals Society of China, 2018, 28: 802−811.

[29] FENG Q, CARROLL L J, POLLOCK T M. Solidification segregation in ruthenium-containing nickel-base superalloys [J]. Metallurgical Materials Transactions A, 2006, 37: 1949−1962.

[30] BRODY H D, FLEMINGS M C. Solute redistribution during dendritic solidification [J]. Transaction AIME, 1966, 236: 615−624.

在不同直径坩埚中定向凝固 Sn−Ni 包晶合金的宏观偏析和热溶质对流引起的雀斑缺陷

彭 鹏[1,2,3]，李升渊[1]，郑万朝[1]，鲁 力[1]，周树东[1]

1. 兰州大学 材料与能源学院，兰州 730000；
2. 兰州大学 磁学与磁性材料教育部重点实验室，兰州 730000；
3. 西北稀有金属研究院，石嘴山 753000

摘　要：与其他合金系不同，本文通过对定向凝固 Sn−Ni 包晶合金中枝晶状糊区的观察发现，雀斑缺陷在包晶反应前后的两个不同区域出现。此外，实验结果证明，枝晶形貌受温度梯度区域熔化效应和 Gibbs−Tbomson 效应的影响。因此，提出考虑上述两种效应及包晶反应的新瑞利数 Ra_{P}。新瑞利数 Ra_{P} 的计算预测结果证实包晶凝固过程中雀斑在两个不同区域形成，且在较大直径的试样中热溶质对流更显著。

关键词：雀斑形成；定向凝固；热溶质对流；枝晶凝固；Sn−Ni 包晶合金

(Edited by Wei-ping CHEN)